"Spectral *a priori*" to "spatial *a posteriori*" in continuous-wave image reconstruction in near-infrared optical tomography

Guan Xu,[a] Daqing Piao,[a]* Hamid Dehghani [b]
[a]School of Electrical and Computer Engineering, Oklahoma State University, Stillwater, OK, USA
[b]University of Birmingham, Birmingham, UK

* School of Electrical and Computer Engineering, Oklahoma State University, Stillwater, OK 74078
(Phone: 405-744-5250; FAX: 405-744-9198; e-mail: daqing.piao@okstate.edu)

ABSTRACT

This work examines the robustness of spectral *prior* to continuous-wave based, with respect to frequency domain based, image reconstruction for unique recovering of chromophores and scattering property distributions. An analytical model for parametric uncertainty in recovering optical property is derived, which afterwards is implemented for optimized selection of wavelengths and quality estimation of the image. Simulation results agree with the theoretical predictions in the following aspects: 1) the proposed analytical model is capable of selecting the optimal set of wavelengths for CW-based spectral reconstruction; 2) with sufficient number of wavelengths, DC-only reconstruction can resolve the concentrations of several important chromophores and scattering parameters, with the accuracy and background artifact level equivalent to those by DC-excluded or DC-included frequency-domain reconstructions; and 3) including DC in frequency-domain reconstruction generally improves reconstruction outcome as compared to when neglecting DC.

Keywords: multi-spectral, optical tomography, image reconstruction

1. INTRODUCTION

The outcome of functional imaging of near-infrared (NIR) optical tomography [1-2] depends upon the information obtained over a spectrum of light. A conventional technique of spectral optical tomography reconstruction is to reconstruct the wavelength-specific absorption and scattering properties first, then to derive the concentrations of tissue chromophores and distributions of the scatterers. An alternative technique of spectral optical tomography reconstruction utilizes *a priori* knowledge of the absorption and scattering spectra of tissue compositions within the NIR range to modify the inverse problem to directly recover the chromophore concentrations and scattering parameters including scattering power and amplitude. Such alternative technique, which is commonly stated as "spectral-*prior*" method, has been demonstrated by a number of studies [1-2]. The most successful demonstration[2] of spectral-*prior* method has been in coupling with *a priori* knowledge of the spatial content of the tissue under frequency-domain imaging, in other words, the *spectral-prior* has been implemented along with *spatial-prior* in frequency-domain measurement.

An interesting question thereby arises, in regards to the outcome of spectral-*prior* without the availability of *spatial-prior*, that what the likelihood of recovering the spatially-resolved spectral information would be, given only continuous-wave measurement. Our study on multi-wavelength optical tomography without *spatial-prior* has shown that implementing the spectral-*prior* in DC measurements often results in spatial information being reconstructed in unexpected level of details. This observation is referred to as "spectral *a priori*" to "spatial *a posteriori*", in other words it is the likelihood of accurately recovering spatially-resolved tissue absorption and scattering distribution from spectral reconstruction without spatial *prior*. The observation that spectrally-resolved measurements in DC lead to accurate spatially-resolved reconstruction, in our opinion, deserves further investigation. This study, as an initial exploration of the underlining mechanism, attempts to justify one derivative issue of such mechanism, specifically the reliability of recovering each unknown spectral variables including chromophore concentrations and scattering contributions under DC-based reconstruction. Based on the analytical approach demonstrated in our previous study [3], the analytical solution for multi-spectral optical tomography and the "parametric reconstruction uncertainty level" (PRUL) of each variable being reconstructed are derived, in a semi-infinite planar medium geometry. Such model provides quantitative means of estimating the relative errors among the parameters subjected to spectral reconstruction, with which the quality of spectral reconstruction may be better understood.

Multimodal Biomedical Imaging VI, edited by Fred S. Azar, Xavier Intes, Proc. of SPIE Vol. 7892,
78920D · © 2011 SPIE · CCC code: 1605-7422/11/$18 · doi: 10.1117/12.873462

In this study the analytical model is first implemented on the optimization of the wavelength sets for the spectral measurements. Studies [1, 4] have demonstrated selection of the optimum wavelengths for reliable recovery of chromophore concentrations and scattering parameters based on statistical investigation, by comparing numerically approximated sensitivity matrices derived from numerous possible wavelength combinations within the NIR spectrum, which is computationally intensive. In this paper, a novel method of optimizing the selection of wavelengths is investigated based on the PRUL model of multi-spectral optical tomography, which is found to be computationally less demanding.

The analytic model introduced in this work also supports the uniqueness of continuous-wave spectral optical tomography, which is an extension of the prediction made in our previous studies for single wavelength optical tomography [3]. The uniqueness of continuous-wave spectral optical tomography substantiated integrating more wavelengths in direct-current measurement to improve spectral reconstruction [1-2, 4-7]. As few studies have investigated the difference in performance between continuous wave and frequency domain spectral optical tomography, this study extends the approach of single-wavelength analysis in [3] to the analysis of spectral-*prior*, on measurement combinations of 1) continuous wave only (DC); 2) frequency domain measurements excluding direct-current components (AC+PHS); and 3) frequency domain measurements including direct-current (DC+AC+PHS), in the outcome of "spatial *a posteriori*" from "spectral *a priori*".

Finally, this study conduct numerical evaluations of synthetic models to examine the effect of "spectral *a priori*" on "spatial *a posterior*". The simulation studies demonstrate that, in agreement with the analytical predictions: 1) the proposed analytical model is capable of selecting the optimum set of wavelengths for spectral reconstruction; 2) with sufficient number of wavelengths for a given set of tissue chromophores, the DC-only reconstruction delivers spatially-resolved chromophore concentrations and scattering parameters with the accuracy and background artifact equivalent to that of AC+PHS and DC+AC+PHS; and 3)including DC in frequency-domain reconstruction generally improves reconstruction outcome more than neglecting DC.

2. THEORY

An earlier study [3] on the parametric-recovery-uncertainty-level (PRUL) has demonstrated an analytic approach of estimating the background artifact level in single-wavelength optical tomography reconstruction. The PRUL analysis in [3] adopted the analytic treatment originally introduced in [8], and in this study this analytic approach is extended to spectral reconstruction. For two field points separated from a source at distances of d_1 and d_2, respectively, in a homogenous diffusive medium, one has:

$$\begin{aligned}
\delta(\lambda) &= \ln\left(\frac{d_2}{d_1}\frac{U_{DC}(d_2,\lambda)}{U_{DC}(d_1,\lambda)}\right) = -\rho\cdot\sqrt{\frac{\mu_a(\lambda)}{D(\lambda)}} \\
\alpha(\lambda) &= \ln\left(\frac{d_2}{d_1}\frac{U_{AC}(d_2,\lambda)}{U_{AC}(d_1,\lambda)}\right) = -\rho\cdot\sqrt{\frac{\mu_a(\lambda)}{2D(\lambda)}\left(\sqrt{1+\frac{\omega^2}{v^2\mu_a^2(\lambda)}}+1\right)} \\
\phi(\lambda) &= \Phi(d_2,\lambda)-\Phi(d_1,\lambda) = \rho\cdot\sqrt{\frac{\mu_a(\lambda)}{2D(\lambda)}\left(\sqrt{1+\frac{\omega^2}{v^2\mu_a^2(\lambda)}}-1\right)}
\end{aligned} \tag{1}$$

where $U_{DC}(d, \lambda)$ $U_{AC}(d, \lambda)$ and $\Phi(d, \lambda)$ are the wavelength-specific amplitude of the direct-current modulated amplitude and phase of the modulation of the intensity measured at distance d from the source, respectively. In equ.(1) $\delta(\lambda)$ $\alpha(\lambda)$ and $\varphi(\lambda)$ are the attenuation of the direct-current (DC), the attenuation of the amplitude modulation (AC) and the phase shift (PHS) accordingly between two detectors placed d_1 and d_2 from the source, $\rho = |d_1 - d_1|$ is the distance between the two detectors, and ω is the angular modulation frequency. Also

$$\begin{aligned}
\mu_a(\lambda) &= \sum_i \varepsilon_i(\lambda)c_i, \\
\mu_s'(\lambda) &= A\lambda^{-b}, \\
D(\lambda) &= 1/3[\mu_a(\lambda)+\mu_s'(\lambda)]
\end{aligned} \tag{2}$$

are the absorption, scattering and diffusion coefficients of the medium at wavelength λ, respectively, where $\varepsilon_i(\lambda)$ is the extinction coefficient of chromophore i at λ and A is the scattering amplitude and b is the scattering power. The PRUL of

the chromophore concentrations and the scattering amplitude/power can be derived by analysis of the propagation of uncertainty and chain rule of partial derivatives as:

$$\sigma_{x_j} = \sqrt{\left(\frac{\partial x_j}{\partial M(\lambda)}\right)^2 \cdot \sigma^2_{M(\lambda)}} = \left|\frac{\partial x_j}{\partial \mu(\lambda)} \cdot \frac{\partial \mu(\lambda)}{\partial M(\lambda)}\right| \cdot \sigma_{M(\lambda)} = \left|\frac{\partial x_j}{\partial \mu(\lambda)}\right| \cdot \sigma_{\mu(\lambda)} \tag{3}$$

where M represents the set of δ, α and φ for the measurement, and x represents the unknowns including derived concentrations of the chromophores, the scattering amplitude and the scattering power. The μ represents the absorption and scattering coefficients in general. Given the extensive analyses of the PRUL of μ_a and μ_s' in [3], the analytical solution of $\sigma_{\mu(\lambda)}$ given in table 2 and table 4 of [3] are directly integrated into equ. (3), with the $\partial x/\partial \mu$ being newly derived.

Equation (2) transforms to a matrix form of

$$\begin{bmatrix} \mu_a(\lambda) \\ \mu_a(\lambda) \\ \vdots \\ \mu_a(\lambda) \end{bmatrix}_{m\times 1} = \begin{bmatrix} \varepsilon_1(\lambda_1) & \varepsilon_2(\lambda_1) & \cdots & \varepsilon_n(\lambda_1) \\ \varepsilon_1(\lambda_2) & \varepsilon_2(\lambda_2) & \cdots & \varepsilon_n(\lambda_2) \\ \vdots & \vdots & \ddots & \vdots \\ \varepsilon_1(\lambda_m) & \varepsilon_2(\lambda_m) & \cdots & \varepsilon_n(\lambda_m) \end{bmatrix}_{m\times n} \times \begin{bmatrix} c_1 \\ c_2 \\ \vdots \\ c_n \end{bmatrix}_{n\times 1} \tag{4}$$

with which one has

$$\frac{\partial \vec{c}_{n\times 1}}{\partial (\vec{\mu}_a)_{m\times 1}} = [(\bar{\varepsilon}^T)_{n\times m}\, \bar{\varepsilon}_{m\times n}]^{-1} (\bar{\varepsilon}^T)_{n\times m} = \begin{bmatrix} \frac{\partial c_1}{\partial \mu_a(\lambda_1)} & \frac{\partial c_1}{\partial \mu_a(\lambda_2)} & \cdots & \frac{\partial c_1}{\partial \mu_a(\lambda_m)} \\ \frac{\partial c_2}{\partial \mu_a(\lambda_1)} & \frac{\partial c_2}{\partial \mu_a(\lambda_2)} & \cdots & \frac{\partial c_2}{\partial \mu_a(\lambda_m)} \\ \vdots & \vdots & \ddots & \vdots \\ \frac{\partial c_n}{\partial \mu_a(\lambda_1)} & \frac{\partial c_n}{\partial \mu_a(\lambda_2)} & \cdots & \frac{\partial c_n}{\partial \mu_a(\lambda_m)} \end{bmatrix}_{n\times m} \tag{5}$$

and then for the terms in PRUL of chromophore concentrations we have:

$$\left(\bar{\sigma}_c\right)_{n\times 1} = \left|\frac{\partial \vec{c}_{n\times 1}}{\partial (\vec{\mu}_a)_{m\times 1}}\right|_{n\times m} \cdot \left(\bar{\sigma}_{\mu_a(\lambda)}\right)_{m\times 1} \tag{6}$$

Note that the scattering power and amplitude are not linearly related as the chromophore concentrations are in equ. (2). The PRULs of these two variables are derived by firstly obtaining:

$$\log \mu_s' = \log A + (-b)\log \lambda \tag{7}$$

then converting equ. (7) to a matrix form of:

$$\begin{bmatrix} \log[\mu_s'(\lambda_1)] \\ \log[\mu_s'(\lambda_2)] \\ \cdots \\ \log[\mu_s'(\lambda_m)] \end{bmatrix}_{m\times 1} = \begin{bmatrix} 1 & \log\lambda_1 \\ 1 & \log\lambda_2 \\ \cdots & \cdots \\ 1 & \log\lambda_m \end{bmatrix}_{m\times 2} \times \begin{bmatrix} \log A \\ (-b) \end{bmatrix}_{2\times 1} \tag{8}$$

which gives the following result:

$$\left(\frac{\partial \log A}{\partial \log \mu_s'(\lambda_i)}\right)_{1\times m} = \frac{1}{m\sum_{i=1}^{m}\log^2(\lambda_i) - [\sum_{i=1}^{m}\log(\lambda_i)]^2} \cdot \left(\begin{bmatrix} \sum_{i=1}^{m}\log^2(\lambda_i) - \log(\lambda_1)\sum_{i=1}^{m}\log(\lambda_i) \\ \sum_{i=1}^{m}\log^2(\lambda_i) - \log(\lambda_2)\sum_{i=1}^{m}\log(\lambda_i) \\ \cdots \\ \sum_{i=1}^{m}\log^2(\lambda_i) - \log(\lambda_m)\sum_{i=1}^{m}\log(\lambda_i) \end{bmatrix}^T \right)_{1\times m} \tag{9}$$

$$\left(\frac{\partial b}{\partial \log \mu_s'(\lambda_i)}\right)_{1\times m} = \frac{1}{m\sum_{i=1}^{n}\log^2(\lambda_i) - [\sum_{i=1}^{n}\log(\lambda_i)]^2} \cdot \left(\begin{bmatrix} \sum_{i=1}^{m}\log(\lambda_i) + m\cdot\log(\lambda_1) \\ \sum_{i=1}^{m}\log(\lambda_i) + m\cdot\log(\lambda_2) \\ \cdots \\ \sum_{i=1}^{m}\log(\lambda_i) + m\cdot\log(\lambda_m) \end{bmatrix}^T \right)_{1\times m} \tag{10}$$

The PRULs of scattering amplitude and power are finally expressed as:

$$\sigma_A = \left|\frac{\partial A}{\partial \log A}\cdot\frac{\partial \log A}{\partial \log \mu_s'(\lambda)}\cdot\frac{\partial \log \mu_s'(\lambda)}{\partial \mu_s'(\lambda)}\right| \cdot \sigma_{\mu_s'(\lambda)} = A\cdot\left|\frac{\partial \log A}{\partial \log \mu_s'(\lambda)}\right| \cdot \frac{\sigma_{\mu_s'(\lambda)}}{\mu_s'(\lambda)} \tag{11}$$

$$\sigma_b = \left|\frac{\partial b}{\partial \log \mu_s'(\lambda)}\cdot\frac{\partial \log \mu_s'(\lambda)}{\partial \mu_s'(\lambda)}\right| \cdot \sigma_{\mu_s'(\lambda)} = \left|\frac{\partial b}{\partial \log \mu_s'(\lambda)}\right| \cdot \frac{\sigma_{\mu_s'(\lambda)}}{\mu_s'(\lambda)} \tag{12}$$

Up to here, by substituting expressions in table 2 and 4 in [3] to equ.s (6) (11) and (12), all the PRUL equation for reconstruction variables in multi-spectral optical tomography are derived and a series of comparison and analysis will be conducted to reveal the intrinsic relationships between the reconstruction parameters. It should also be noted that since PRUL analysis is expressed in terms of the standard deviations, all comparisons will neglect common factors and consider only the absolute values of the equations.

Integrating the results of PRUL in the previous study, the uncertainty level of the parameters to be recovered can be quantitatively compared. Note that in equ. (5), the expression does not facilitate the normalization of σ_{μ_a} on the right hand side compared to the ($\sigma_{\mu_s'}/\mu_s'$) terms in equ.s (9) and (10). Multiplication by μ_a values is thereby necessary when utilizing (σ_{μ_a}/μ_a) results.

It is desirable that the uncertainty values can be reduced by correctly selecting the wavelengths used in the system. One approach is to increase absolute value of the determinant of $\varepsilon^T\varepsilon$ in equ. (6) and $m\sum_{i=1}^{m}\log^2(\lambda_i) - [\sum_{i=1}^{m}\log(\lambda_i)]^2$ in equ.s (9) and (10) to reduce the overall absolute value of the PRULs. Several random attempts on the denominator terms will show that the values of $\left|m\sum_{i=1}^{m}\log^2(\lambda_i) - [\sum_{i=1}^{m}\log(\lambda_i)]^2\right|$ stay in a narrow range of [0,1] but the determinant of $\varepsilon^T\varepsilon$ varies in several orders depending on the selection of wavelengths. Such phenomenon is understandable because high similarity between the row vectors of the extinction coefficient matrix could induce rank deficiency, making its determinant close to zero or producing singular values in its pseudo-inverse, which reduces the accuracy of matrix inversion in equ. (4). Previous study [1] has shown such problems and recommended to construct sensitivity matrix with small residual numbers for improving the reliability of the inverse algorithm. From another perspective, the determinant of the matrix geometrically quantifies the volume in the space bounded by the row factors, therefore, larger divergence of the row vectors in extinction coefficients enclosures larger volumes in the vector space, which again supports the hypothesis that larger determinant of the $\varepsilon^T\varepsilon$ matrix ensures more accurate reconstruction.

Further, reference [4] indicates that the uniformity of the sensitivity matrix (∂x/∂ M(λ) in equ. (3)) is also desired for stable and accurate reconstruction. The criteria for wavelengths optimization in this study thereby also include the standard deviation of (∂x/∂ M(λ)) for each wavelength set and again the common terms $|\partial\mu(\lambda)/\partial M(\lambda)|\cdot\sigma_{M(\lambda)}$ is neglected in the quantitative evaluation.

This study is conducted for 3 sets of wavelength, each containing 5 wavelengths adopted from a previous literature [1], in the numerical evaluation of the analytical approach for recovering concentrations of oxygenated hemoglobin, deoxygenated hemoglobin, water, scattering power, and scattering amplitude, as is listed in table 1. Although the previous study [1] has shown that the wavelength selection method is capable of determining the optimum wavelength set and validated the method with simulations, it is difficult to rank the performance of the other two sets. In observation of Table 1 as well as the expectation to have larger denominator determinant and smaller variation among the sensitivity values, the performance ranking of the three wavelength sets can be predicted, from best to worst as: 3,1,2, which agrees with the simulations presented in[1]. Validations from more aspects will be shown later in this paper.

For the calculation of the PRULs in this study, the chromophore concentrations and scattering parameters are estimated as: $C_{HbO}=C_{Hb}=0.01$mM, $C_{H_2O}=40\%$ and A=b=1. It is also assumed that for all measurement types the relative uncertainties of the measurements are the same, that is: $\frac{\sigma^2_{\delta(\lambda)}}{\delta^2(\lambda)}=\frac{\sigma^2_{\alpha(\lambda)}}{\alpha^2(\lambda)}=\frac{\sigma^2_{\phi(\lambda)}}{\phi^2(\lambda)}$. Further, with a given set of wavelengths and a modulation frequency, equ.(1) implicitly determined the value of $\frac{\alpha^2(\lambda)+\phi^2(\lambda)}{\alpha^2(\lambda)-\phi^2(\lambda)}$ ($=\sqrt{1+\frac{\omega^2}{v^2\mu_a^2(\lambda)}}$), which is approximately 1 for all cases. With these approximations and preconditions in-place, equ.s (6) (11) and (12) can be evaluated and compared to simulation results later in this paper.

Table 1 Wavelength sets to be examined and comparison of the PRUL evaluation with the analytical solutions

Set	Wavelengths / nm	Absorption component		Scattering component	
		Determinant of denominator: $(\varepsilon^T\varepsilon)^{-1}$	Standard deviation of chromophores dev(ε)	Absolute value of denominator	Sensitivity standard deviation of scattering amplitude and power
1	740,788,866,902,926	8.18×10^{-7}	63.7	0.18	1.03
2	650,700,716,860,890	2.58×10^{-7}	388.0	0.37	0.67
3	650,716,866,914,930	1.30×10^{-5}	63.8	0.53	0.45

3. SIMULATIONS

Simulations are conducted to quantitatively examine the accuracy of the analytically derived predictions. Similar to [3], PRULs of three measurement types: DC, AC+PHS, DC+AC+PHS are calculated and compared.

3.1 Synthetic model

Forward model is carried out with Finite Element Method solution of photon diffusion at each wavelength[9]:

$$\left(-\frac{\mu_a(\vec{r},\lambda)}{D(\vec{r},\lambda)}+\frac{i\omega}{vD(\vec{r},\lambda)}\right)U(\vec{r},\omega,\lambda)+\nabla^2U(\vec{r},\omega,\lambda)=-\frac{S(\vec{r},\omega,\lambda)}{D(\vec{r})} \tag{13}$$

Where $U(\vec{r},\omega,\lambda)$ is the photon fluence of wavelength λ modulated to angular frequency ω (ω=0 for DC) at position $\vec{r}$ in phasor notation. $S(\vec{r},\omega,\lambda)$ is the source term. The Jacobian matrix is constructed according to the measurement type [3] as:

$$J=\begin{bmatrix}DC\\AC\\PHS\end{bmatrix}=\begin{bmatrix}\frac{\partial\ln U_{DC}(\lambda_1)}{\partial x} & \frac{\partial\ln U_{DC}(\lambda_2)}{\partial x} & \cdots & \frac{\partial\ln U_{DC}(\lambda_m)}{\partial x}\\ \frac{\partial\ln|U_{AC}(\lambda_1)|}{\partial x} & \frac{\partial\ln|U_{AC}(\lambda_2)|}{\partial x} & \cdots & \frac{\partial\ln|U_{AC}(\lambda_m)|}{\partial x}\\ \frac{\partial\Phi_{AC}(\lambda_1)}{\partial x} & \frac{\partial\Phi_{AC}(\lambda_2)}{\partial x} & \cdots & \frac{\partial\Phi_{AC}(\lambda_m)}{\partial x}\end{bmatrix} \tag{14}$$

where x represents the parameters to be reconstructed, including chromophore concentrations and scattering amplitude and scattering power. The Levernberg-Marquardt algorithm is implemented as the inverse solver.

A 43mm-radius circular geometry with 16 optode channels evenly distributed on its perimeter is used in this study for its relatively uniform sensitivity along the azimuthal direction with respect to the center of the circle. Each channel functions as source channel sequentially while others function as detector simultaneously. Background values of each reconstruction variables are assigned identical to those used in analytical calculation and the contrast of the anomaly are: C_{HbO_anom} =0.0023mM, C_{Hb_anom} = 0.0023mM, $C_{H_2O\_anom}$ =80% A_{anom}=2, and b_{anom}=2. Contrasts of each of the five variables are assigned to a set of five 8mm-radius targets, as is shown in Fig.1 columns Set. The targets locate 25 mm away from the center of the geometry with 0.4π angular separation. 1% randomly distributed noise is added to all forward data to simulate the perturbations in the actual measurement system.

3.2 Results

Fig.1 shows the reconstruction results and Table 2 demonstrates the maximum values of each variable within the target regions and the percentage error of the contrast. Comparisons in Fig. 1 and table 2 infer that the set 3 outperforms the other two in terms of the overall reliability of quantitative reconstruction and the crosstalk among the recovered variables. Next to the set 3 is set 1, which underestimates hemoglobin concentration and has higher level of crosstalk between hemoglobin and scattering parameters in DC reconstruction. The set 2 is the least accurate, producing severe crosstalk between the oxygenated hemoglobin and water concentration. Besides the comparison among the sets of wavelength, it is also noted that for most cases, DC reconstruction demonstrates the most accurate recovery of the targets when the target presents the contrast of only one parameter, and including DC measurement in frequency domain usually improve the estimation precision.

Further, table 3 lists the analytical PRULs and the reconstructed background artifact levels normalized by the absolute variable of the contrast being recovered, which is, in a more explicit way, the inverse of the contrast-noise-ratio. For more clarity in comparison, the noise to contrast (NCR) ratios are normalized by that of the deoxygenated hemoglobin for the absorptive chromophores and by that of the scattering amplitude for the scattering parameters.

Although the analytically estimated values of the noise to contrast ratios always exceed those calculated from the numerical simulations, the data unanimously shows that, $NCR_{c\_Hb} < NCR_{c\_HbO} < NCR_{c\_H_2O}$ for the absorption part and $NCR_A < NCR_b$ for the scattering part, both of which are in agreement with the previous hypotheses. The quantitative inaccuracy could relate to the smoothing effect of the piecewise reconstruction algorithm.

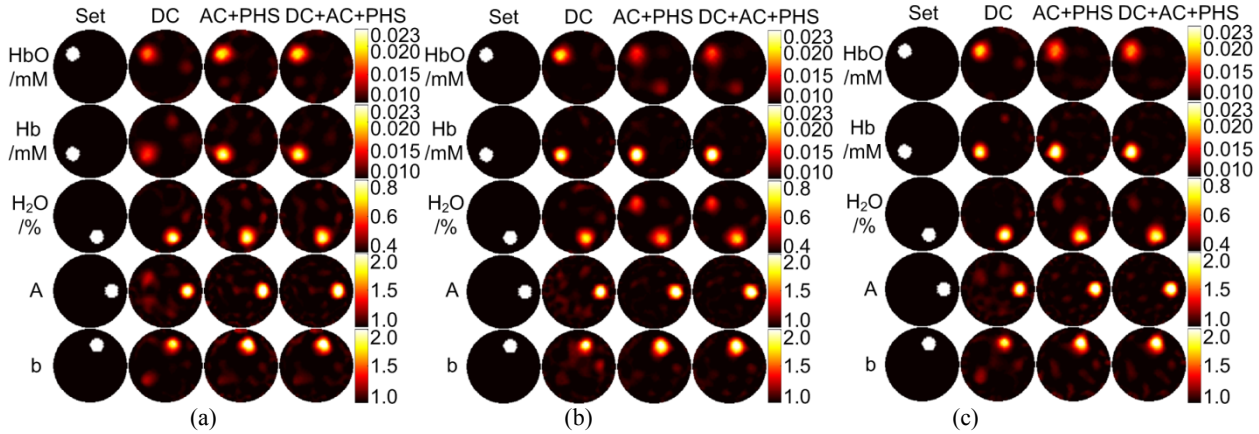

Fig.1Synthetic study on targets with independent contrast

Table 2 Target accuracy comparison

Data		HbO / mM		Hb / mM		H2O / %		A		b	
		Abs.	Err. / %	Abs.	Err. / %	Abs.	Err. / %	Abs.	Err. / %	Abs.	Err. / %
Set Values		2.3E-2		2.3E-2		0.80		2.0		2.0	
(1)	DC	1.7E-2	-46	1.6E-2	-55	0.82	5	2.2	21	1.9	-9
	AC+PHS	2.0E-2	-23	2.3E-2	-2	0.81	2	2.4	39	2.3	30
	DC+AC+PHS	2.0E-2	-24	2.2E-2	-6	0.80	0.4	2.3	34	2.2	23
(2)	DC	2.0E-2	-21	2.4E-2	4	0.72	-21	2.4	40	2.1	7
	AC+PHS	1.6E-2	-56	2.6E-2	24	0.67	-33	2.3	26	2.1	6
	DC+AC+PHS	1.7E-2	-48	2.7E-2	27	0.69	-27	2.2	23	2.1	10
(3)	DC	2.0E-2	-25	2.3E-2	1	0.83	8	2.3	33	1.9	-11
	AC+PHS	1.8E-2	-42	2.5E-2	16	0.78	-6	2.4	45	2.2	19
	DC+AC+PHS	1.8E-2	-39	2.5E-2	18	0.77	-8	2.4	39	2.2	17

Table 3 Comparison between the PRULs and the background artifact levels normalized by variable contrast

Set		Measurement	HbO / mM		Hb / mM		H2O / %		A		b	
			Abs.	Norm.	Abs.	Norm.	Abs.	Norm.	Abs.	Norm.	Abs.	Norm.
(3)	Ana.	DC	5.38	5.40	1.00	1	3.24	3.26	0.79	1	3.10	3.91
		AC+PHS	7.61	5.40	1.41	1	4.59	3.26	1.12	1	4.39	3.91

		DC+AC+PHS	13.17	5.40	2.44	1	7.94	3.26	1.12	1	4.39	3.91
	Sim.	DC	0.0489	1.89	0.0258	1	0.0395	1.53	0.0260	1	0.0381	1.46
		AC+PHS	0.0716	1.62	0.0443	1	0.0466	1.05	0.0242	1	0.0498	2.06
		DC+AC+PHS	0.0521	1.58	0.0328	1	0.0367	1.12	0.0203	1	0.0404	1.99

4. DISCUSSIONS AND CONCLUSION

The predictions made by a novel analytical PRUL model regarding spectral *a priori* leading to spatial *a posteriori* is supported by the results from simulation. The wavelength ranking method shows agreement with previous study, with much less computational intensity. The PRUL values qualitatively estimates the background artifact level of the DC and frequency domain reconstructions, although neglecting DC components in DC+AC+PHS induces explainable aberration. Comparisons on both the multi-spectral tomography reconstruction PRULs and the projected absorption and scattering reconstruction PRULs support the reliability of the model predictions. However, quantitative inaccuracy still exists in the comparisons, which could be attributed to the approximation and smoothing effect of the inverse algorithm.

An interesting observation is that different from the study in [3], the DC reconstruction with spectral *prior* has quite desirable reconstruction outcome. This should relate to the expectation that sufficient wavelength components will impose the outcome as a result of the uniqueness of DC multispectral tomography, with minimized cross-coupling among the parameters to be recover. Moreover, fewer measurement components facilitate less system noise in the inverse problem and thereby generate less background artifacts, improving the overall DC reconstruction quality. As to frequency domain reconstruction, although DC component could contribute to excessive reconstruction uncertainty, its extra information has actually balanced the negative effect and made DC+AC+PHS a better choice.

ACKNOWLEDGEMENT

This work has been supported in part by the Prostate Cancer Research Program of the U.S. Army Medical Research Acquisition Activity (USAMRAA) through grants #W81XWH-07-1-0247 and #W81XWH-10-1-0836.

REFERENCES

[1] Corlu, A., et al., "Diffuse optical tomography with spectral constraints and wavelength optimization," Appl. Opt. 44(11), 2082-2093 (2005)
[2] Srinivasan, S., et al., "Spectrally constrained chromophore and scattering near-infrared tomography provides quantitative and robust reconstruction," Appl. Opt. 44(10), 1858-1869 (2005)
[3] Xu, G., et al., "Direct-current-based image reconstruction versus direct-current included or excluded frequency-domain reconstruction in diffuse optical tomography," Appl. Opt. 49(16), 3059-3070 (2010)
[4] Eames, M.E., et al., "Wavelength band optimization in spectral near-infrared optical tomography improves accuracy while reducing data acquisition and computational burden," Journal of Biomedical Optics 13(5), 054037-9 (2008)
[5] Li, C., et al., "Multispectral diffuse optical tomography with absorption and scattering spectral constraints," Appl. Opt. 46(34), 8229-8236 (2007)
[6] Jones, P.B., et al., "Simultaneous multispectral reflectance imaging and laser speckle flowmetry of cerebral blood flow and oxygen metabolism in focal cerebral ischemia," Journal of Biomedical Optics 13(4), 044007 (2008)
[7] Xu, H., et al., "Magnetic-resonance-imaging-coupled broadband near-infrared tomography system for small animal brain studies," Appl. Opt. 44(11), 2177-2188 (2005)
[8] Fantini, S., et al., "Quantitative determination of the absorption spectra of chromophores in strongly scattering media: a light-emitting-diode based technique," Appl. Opt. 33(22), 5204-5213 (1994)
[9] Dehghani, H., et al., "Near infrared optical tomography using NIRFAST: Algorithm for numerical model and image reconstruction," Communications in Numerical Methods in Engineering 25(6), 711-732 (2009)